Performance Analysis of Underwater RSMA-Assisted Covert Wireless Communications

Xuquan Luo, Liang Yang, *Senior Member, IEEE*, George C. Alexandropoulos, *Senior Member, IEEE*, Jules M. Moualeu, *Senior Member, IEEE*, and Xi Yang, *Member, IEEE*

***Abstract*—This paper investigates the covert communication performance of a radio frequency underwater acoustic communication (RF-UAC) system deploying rate-splitting multiple access (RSMA). The proposed system aims to enhance the covertness of communication signals while maintaining reliable communications for legitimate users. In this context, we model the RF link using the Rayleigh distribution and the UAC link using the $\kappa - \mu$ shadow distribution. Moreover, We analytically evaluate key performance metrics for the proposed system, including the detection error probability, outage probability and covert communication rate under various system parameters, such as signal-to-noise ratio thresholds and power allocation between public and private streams. Our extensive numerical investigations validate the proposed analytical expressions, demonstrating the role of key system and channel parameters on the performance of RSMA-assisted RF-UAC communications.**

***Index Terms*—Covert communication, detection error probability, outage probability, rate-splitting multiple access, κ-μ shadowed distribution, underwater acoustic communications.**

I. Introduction

With the emergence of sixth-generation (6G) wireless communication technologies, the demand for ultra-reliable, low-latency, and secure communication systems has intensified [1]. On this matter, the integration of terrestrial and underwater communication networks is poised to play a critical role in supporting diverse applications, including environmental monitoring, resource exploration, and military operations [2]. In the context of 6G networks, relay systems are a key enabler, providing a practical solution to extend coverage and enhance the reliability of communication systems, especially in integrated land-underwater communication networks. These systems enable the transmission of signals across difficult environments, improving communication efficiency while mitigating the effects of signal degradation. They are especially critical for addressing the challenges posed by underwater communication, where direct transmission is often impractical due to severe attenuation and environmental interference [3], [4], [5].

Underwater communications can be realized with acoustic, optical, and radio frequency (RF) signals [6].

Among these, acoustic communication is the most widely used due to its long propagation distance and strong penetration capabilities. Typically, underwater acoustic links support communication over distances up to tens of kilometers, with data rates below 100 kbps due to limited bandwidth and severe multipath fading [7]. In contrast, underwater optical wireless communication (UOWC) can achieve data rates exceeding 10 Mbps over short distances ($<$100 meters), but suffers from high attenuation and scattering in turbid water [8], [9]. While underwater RF communication offers moderate data rates (100 kbps–few Mbps) over short distances (typically $<$10 meters), and is severely attenuated in conductive seawater due to high permittivity and conductivity [10], [11]. Recently, the performance of underwater communications under various wireless conditions modeled using versatile fading distributions such as the $\mathcal{K}$-distribution [12], $\kappa - \mu$ shadowed distribution [13], [14], $\alpha - \mathcal{F}$-distribution [15], has attracted significant attention in the research community.

With the ever-increasing demand for high-speed and ultra-reliable wireless communications, the need to ensure the security and privacy of data in underwater communications has gained momentum [16]. In this context, covert communication has emerged as a critical area of research. Unlike traditional encryption techniques which are designed to protect data transmission, covert communication operates at the physical layer to ensure undetectability, thus enhancing system security and privacy in sensitive scenarios [17], [18]. Despite its promise, achieving a balance between covertness and reliability remains a significant challenge in complex wireless environments characterized by multipath fading, noise interference, and other impairments [19], [20].

Received 25 February 2025; revised 28 May 2025 and 5 August 2025; accepted 24 September 2025. Date of publication 6 October 2025; date of current version 23 December 2025. This work was supported by the National Natural Science Foundation of China under Grant 62272153, Grant U23A20278, and Grant 62161012. The associate editor coordinating the review of this article and approving it for publication was H. Jung. *(Corresponding author: Liang Yang.)*

Xuquan Luo is with the College of Computer Science and Electronic Engineering, Hunan University, Changsha 410082, China (e-mail: luoxuquan@hnu.edu.cn).

Liang Yang is with the College of Computer Science and Electronic Engineering, Hunan University, Changsha 410082, China, also with the School of Communication and Electronic Engineering, Jishou University, Jishou 416000, China (e-mail: liangy@hnu.edu.cn).

George C. Alexandropoulos is with the Department of Informatics and Telecommunications, National and Kapodistrian University of Athens, 15784 Athens, Greece (e-mail: alexandg@di.uoa.gr).

Jules M. Moualeu is with the University of the Witwatersrand, Johannesburg 2000, South Africa, and also with the School of Energy Systems, Lappeenranta-Lahti University of Technology, 53850 Lappeenranta, Finland (e-mail: jules.moualeu@wits.ac.za).

Xi Yang is with the School of Communication and Electronic Engineering, Jishou University, Jishou 416000, China (e-mail: ynkej@163.com).

Digital Object Identifier 10.1109/TCOMM.2025.3618170

To address these challenges, recent advancements have explored the integration of rate-splitting multiple access (RSMA) into covert communication frameworks across diverse network scenarios. In [21], the authors presented a comprehensive survey of physical layer security in RSMA systems, emphasizing the influence of common stream power allocation and successive interference cancellation (SIC) decoding order in mitigating both internal and external eavesdropping threats. In [22], an RSMA-assisted uncrewed aerial vehicle (UAV) communication framework was proposed, wherein a joint optimization of the UAV trajectory, transmit power, and rate allocation enhances energy efficiency and user fairness compared to conventional multiple access techniques. Extending this work, the authors in [23] derived closed-form ergodic capacity expressions for RSMA-enabled UAV networks and demonstrated that system capacity can further be boosted by strategically optimizing the UAV's hovering position. In [24], the authors formulated a max-min optimization problem to maximize the minimum covert rate in multi-antenna RSMA systems, revealing a superior performance over space division multiple access (SDMA) and non-orthogonal multiple access (NOMA) across varying load conditions. In [25], a secure RSMA communication was investigated through a jamming-based covert technique that simultaneously maximizes the user rate while satisfying covertness constraints. Furthermore, the work of [26] investigated the covert performance and physical layer security performance of an uplink simultaneously transmitting and reflecting reconfigurable intelligent surface-assisted semi-grant-free-NOMA system in the presence of illegitimate users. Similarly, the work of [27] explored RSMA-assisted ambient backscatter systems and revealed that RSMA provides higher covert rates and stronger detection error performance than NOMA, albeit at the cost of increased outage probability under certain interference conditions. Lastly, in the underwater environment, the authors in [28] investigated RSMA-enabled multi-user UOWC systems, where a novel resource optimization strategy was proposed over an exponential-generalized gamma (EGG) turbulence channel with pointing errors. Moreover, the study demonstrated that RSMA can substantially improve ergodic capacity performance in such highly impaired environments.

A. Motivation and Contributions

Covert communication over underwater acoustic channels has recently gained traction due to its applications in maritime surveillance, underwater exploration, and unmanned underwater equipment. As a result, several works in the exiting literature have explored the concept of covertness in the context of underwater acoustic communication. For example, in [29], an autonomous underwater vehicle-assisted underwater acoustic communication (UAC) covert architecture was proposed to optimize the energy use and throughput. In [30], a chaos-based UAC scheme using ship-radiated noise was proposed. In parallel, covert communication strategies have also been studied in relay-based systems, such as collaborative jamming and relay selection [31], and full-duplex relay architectures [32].

Although covert communication and RSMA have been independently explored in both underwater and terrestrial environments, their integration in heterogeneous relay systems—particularly over mixed RF–UAC links—has received little attention. In such land-sea scenarios, relay-based RF-UAC architectures are commonly adopted due to the distinct propagation characteristics of radio and acoustic channels.

To better highlight the research gap in the open literature, Table I summarizes recent studies on RSMA-assisted covert and underwater communication systems and the novelty of our work with the current state-of-the-art. It is evident from the table that existing works vary in their focus on RSMA, channel modeling, and performance evaluation. However, none of the them has considered an RSMA-enabled covert communication over dual-hop RF–UAC links under practical underwater fading conditions, which is the focus of this paper.

Motivated by the preceding discussion, this paper proposes a novel RSMA-assisted dual-hop RF-UAC covert communication system wherein the RF hop is modeled using Rayleigh fading for analytical tractability and its adequacy in typical terrestrial scenarios, while the UAC hop adopts the $\kappa-\mu$ shadowed fading model due to its excellent agreement with empirical underwater measurements. In this context, we investigate the system performance in terms of the detection error probability (DEP), outage probability (OP), and covert rate (CR). The main contributions of this work are summarized as follows:

- We introduce an RSMA-assisted RF-UAC covert communication model, combining Rayleigh fading for the RF link and $\kappa-\mu$ shadowed fading for the UAC link.
- We analyze the performance of the proposed system by deriving closed-form expressions of the DEP, OP and CR. To provide useful insights into the impact of various system parameters on the covert performance, we subsequently derive their corresponding asymptotic expressions at high signal-to-noise ration (SNR).
- We provide Monte Carlo simulations to validate the accuracy of the proposed theoretical framework and investigate how various parameters affect the CR and other performance indicators in realistic land-to-sea scenarios.

B. Organization

The rest of the paper is organized as follows. In Section II, we present the system and channel models that form the foundation for our analysis. This section provides a detailed description of the system architecture, including the RSMA-assisted RF-UAC model, as well as the channel conditions for both the RF and UAC links. Section III provides the theoretical framework for the key performance metrics, including DEP, OP, and CR. Section IV extends the analysis of the OP to the general case where the $\kappa-\mu$ shadowed fading parameters *m* and μ take arbitrary real values. In Section V, the numerical results are presented followed by a thorough discussion of the findings, that offers some important performance insights under different system parameters. Finally, Section V provides

TABLE I
SUMMARY OF RELATED WORKS ON RSMA-ASSISTED COVERT OR UNDERWATER COMMUNICATION SYSTEMS

Ref	RSMA	Channel Model	Covert Communication	Metrics	Asymptotic Analysis
[3]	✘	Rician + κ-μ Shadowed (RF-UAC)	✘	OP, ABER, ACC	✔ (OP, ABER)
[26]	✘ (NOMA)	Rayleigh (STAR-RIS)	✔	DEP, OP, SOP	✘
[27]	✔	Rayleigh	✔	DEP, OP, CR	✔ (OP)
[28]	✔	EGG (UOWC)	✘	Ergodic Capacity	✘
[33]	✘ (NOMA)	Rayleigh (STAR-RIS)	✔	DEP, OP, ECR	✘
Our Work	✔	Rayleigh + κ-μ Shadowed (RF-UAC)	✔	DEP, OP, CR	✔ (DEP, OP)

Note: ✔ : considered; ✘: not considered.

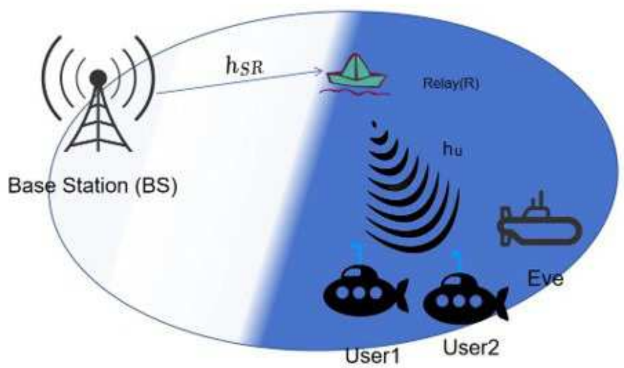

Fig. 1. The considered RSMA-assisted RF-UAC communication system.

some concluding remarks through a brief summary of key findings of this work, and suggest some research directions as potential avenues for future work for the advancement of the state-of-the-art.

II. SYSTEM MODEL

The RSMA-assisted RF-UAC communication system considered in this work is illustrated in Fig. 1. The proposed system consists of a land base station (BS), a sea buoy relay station (R), two legitimate underwater users (User1 denoted by U_1 and User2 denoted by U_2), and an underwater eavesdropper (Eve). It is assumed that each node is equipped with a single antenna. Due to distance and environmental barriers, there is no direct connection between BS and U_1, U_2, or Eve. Both h_{SR} and h_u have already been defined after eqns. (1) and (2).

As a result, RF signals are transmitted from the BS to R in the fist time slot. In the second time slot, R converts the received RF signals into acoustic signals and transmits them to the underwater users over the UAC links using the amplify-and-forward (AF) protocol. Specifically, with the help of RSMA, the user information is divided into two parts: public and private. The public information is shared between the two legitimate users, while the private information is user-specific. Messages M_1 and M_2 are intended for users U_1 and U_2, respectively. Each message is divided into two components: namely, a common part denoted as M_1^c and M_2^c, which can be decoded by both users, and a private part identified as M_1^p and M_2^p, intended only for the respective user. The public information is jointly encoded into a common stream x_c, while the private parts are separately encoded into streams x_1 and x_2 intended for U_1 and U_2, respectively.

We assume that the transmit powers of the common message stream x_c and the private message streams x_1 and x_2 at the BS are denoted by P_c, P_1, and P_2, respectively. The total transmit power P_S is distributed among the streams as follows: $P_c = \alpha_c P_S$, $P_1 = \alpha_1 P_S$, and $P_2 = \alpha_2 P_S$, where α_c, α_1, and α_2 are the power allocation factors satisfying the conditions $\alpha_c + \alpha_1 + \alpha_2 = 1$ and $0 \leq \alpha_c, \alpha_1, \alpha_2 \leq 1$. The power allocated to each message stream ensures the proper transmission of information. Specifically, BS transmits the mixed signals corresponding to the common and private streams to the relay station, which then forwards the signals to the underwater users.

A. The RF Link

For the first hop, the baseband received signal at R can be formulated as

$$y_R = h_{SR} x_s + n_1, \tag{1}$$

where h_{SR} represents the channel gain of the RF link between the source and relay and $x_s = \sqrt{\alpha_c P_S} x_c + \sqrt{\alpha_1 P_S} x_1 + \sqrt{\alpha_2 P_S} x_2$ represents the symbol transmitted by the information source. Additionally, $n_1 \sim \mathcal{CN}(0, \sigma_1)$ represents the complex additive Gaussian white noise (AWGN). We consider Rayleigh fading condition [33] and let $X = |h_{SR}|^2$; therefore, the probability density function (PDF) and the cumulative distribution function (CDF) of X are given by $f(x) = \lambda e^{-\lambda x}$ and $F(x) = 1 - e^{-\lambda x}$, respectively with $\lambda = \frac{1}{\mathbb{E}(X)}$, where $\mathbb{E}(\cdot)$ represents the expectation operation.

B. The UAC Link

For the second hop, the relay operating under AF protocol, first converts the RF signals into acoustic signals and subsequently forwards them to the legitimate the users. The signal received at users can be represented as

$$\begin{aligned} y_U &= \sqrt{P_R} G h_u y_R + n_2 \\ &= \sqrt{P_R} G h_{SR} h_u x_s + \sqrt{P_R} G h_u n_1 + n_2, \end{aligned} \tag{2}$$

where G and P_R denote the amplification coefficient and its transmit power at R, respectively, h_u signifies the channel coefficient of the UAC link and $n_2 \sim \mathcal{CN}(0, \sigma_2)$ is the AWGN. The instantaneous SNR of the UAC link can be expressed as $\gamma_u = \bar{\gamma}_u |h_u|^2$, where $\bar{\gamma}_u = \frac{P_R}{\sigma_2}$ indicating the average SNR of the UAC link. Let $Y = \gamma_u$, and we can obtain the PDF of Y, which has been developed in [34, Eq. (6)], and κ, μ, m, M in [34, Eq. (6)] are the relevant parameters where κ denotes the ratio of main to scattered waveform power,

μ represents the number of multipath clusters, m quantifies the extent of the shadow fading attenuation and *M* captures the expected signal power accounting for factors such as path loss.

III. Performance Analysis

With the system and channel models defined, we now proceed to analyze the key performance metrics that characterize covert communication. In this section, we derive analytical expressions for detection error probability, outage probability, and covert rate, providing a theoretical framework to assess system behavior under various parameters. To begin with, we derive closed-form expressions of the above-mentioned performance metrics. Furthermore, asymptotic analyses are provided to offer clearer insights into system behavior at high SNR.

A. Detection Error Probability

An important performance metric in covert communication systems is the DEP which captures the detectability of the covert transmission and is critical to evaluating system-level covertness. According to [35], the DEP for covert communication is evaluated under two assumptions, H_0 and H_1, where H_0 denotes a scenario where no covert transmission occurs and only normal messages being transmitted, and H_1 denotes a scenario where a covert transmission. Thus, based on the two hypotheses H_0 and H_1, the DEP ξ can be expressed as

$$\xi = P_{FA} + P_{MD}, \tag{3}$$

where P_{FA} denotes the probability of false alarms (under H_0 condition), and P_{MD} denotes the probability of missed detection (under H_1 condition). It is important to note that ξ satisfies the inequality $0 \le \xi \le 1$. Specifically, $\xi = 0$ means that Eve can always accurately detect the covert communication between the transmitting BS and the covert user, while $\xi = 1$ means that Eve is unable to detect any covert transmission. Under both hypotheses, the signal received at Eve can be expressed as

$$\begin{aligned} H_0: y_E &= \sqrt{P_R} G h_{SR} h_u \left(\sqrt{\alpha_c P_S} x_c + \sqrt{\alpha_2 P_S} x_2\right) \\ &\quad + \sqrt{P_R} G h_u n_1 + n_2, \end{aligned} \tag{4}$$

$$\begin{aligned} H_1: y_E &= \sqrt{P_R} G h_{SR} h_u \left(\sqrt{\alpha_c P_S} x_c + \sqrt{\alpha_1 P_S} x_1 \right. \\ &\quad \left. + \sqrt{\alpha_2 P_S} x_2\right) + \sqrt{P_R} G h_u n_1 + n_2. \end{aligned} \tag{5}$$

The average received power at Eve is given by

$$P_E = \begin{cases} P_S P_R G^2 \left|h_{SR}\right|^2 h_u^2 \left(\alpha_c + \alpha_2\right) + P_R G^2 h_u^2 \sigma_1 & \\ +\sigma_2, & H_0 \\ P_S P_R G^2 \left|h_{SR}\right|^2 h_u^2 + P_R G^2 h_u^2 \sigma_1 + \sigma_2, & H_1 \end{cases} \tag{6}$$

The probability of false alarm P_{FA} and the probability of missed detection P_{MD} are given respectively by

$$\begin{aligned} P_{FA} = \Pr\Big[&P_S P_R G^2 \left|h_{SR}\right|^2 h_u^2 \left(\alpha_c + \alpha_2\right) \\ &+ P_R G^2 h_u^2 \sigma_1 + \sigma_2 > \gamma_{\text{th}}\Big], \end{aligned} \tag{7}$$

$$P_{MD} = \Pr\left[P_S P_R G^2 \left|h_{SR}\right|^2 h_u^2 + P_R G^2 h_u^2 \sigma_1 + \sigma_2 < \gamma_{\text{th}}\right], \tag{8}$$

where γ_{th} denotes the detection threshold adopted at the Eve. Then using [36, Eq. (3.451.1)], [36, Eq. (8.352.1)], and [36, Eq. (3.471.9)], we can derive P_{FA} and P_{MD} in closed form, as shown at the bottom of the next page, where $(\cdot)_x$ represents the Pochhammer function, $\Gamma(\cdot)$ is the standard gamma function, and $K_v(\cdot)$ denotes the modified Bessel function of the second kind, $v_1 = k_2 + 1$, $v_2 = k_2 + k_3 + 1$, $B = \frac{m\mu^2(1+\kappa)}{(\mu\kappa+m)\bar{\gamma}_u M}$, and $D = \frac{\mu(1+\kappa)}{\bar{\gamma}_u M}$.

Proof: See Appendix A.

Remark 1: When $\alpha_c = 0$, the base station no longer transmits a common message stream to the users, simplifying the RSMA-based covert transmission system into a NOMA-based covert transmission system. Under this scenario, the value of P_{MD} remains unchanged, while the P_{FA} decreases. Consequently, since $\xi = P_{FA} + P_{MD}$, the DEP of the NOMA system is lower than that of the RSMA system. This result indicates that adopting an RSMA system can enhance the performance of covert communications.

Remark 2: To make the expression more concise, consider that at high SNR, we have

$$P_{FA}^{Asy} \to \Pr\left[P_S P_R G^2 \left|h_{SR}\right|^2 h_u^2 \left(\alpha_c + \alpha_2\right) + \sigma_2 > \gamma_{\text{th}}\right], \tag{11}$$

and

$$P_{MD}^{Asy} \to \Pr\left[P_S P_R G^2 \left|h_{SR}\right|^2 h_u^2 + \sigma_2 < \gamma_{\text{th}}\right]. \tag{12}$$

By using [36, Eq. (3.471.9)], we can further express the asymptotic expressions in (16) and (12) as

$$\begin{aligned} P_{FA}^{Asy} \to\, & Q_1 \left(\frac{\gamma_{th}\text{-}\sigma_2}{\lambda P_S G^2 \left(\alpha_1 + \alpha_2\right) B}\right)^{\frac{v_1}{2}} K_{v_1}\left(2\sqrt{\frac{B\left(\gamma_{th}\text{-}\sigma_2\right)}{\lambda P_S G^2 (\alpha_1 + \alpha_2)}}\right) \\ & - Q_2 \left(\frac{\gamma_{th}\text{-}\sigma_2}{\lambda P_S G^2 \left(\alpha_1 + \alpha_2\right) D}\right)^{\frac{v_2}{2}} K_{v_2}\left(2\sqrt{\frac{D\left(\gamma_{th}\text{-}\sigma_2\right)}{\lambda P_S G^2 (\alpha_1 + \alpha_2)}}\right), \end{aligned} \tag{13}$$

and

$$\begin{aligned} P_{MD}^{Asy} \to 1 &- Q_3 \left(\frac{\gamma_{th}\text{-}\sigma_2}{\lambda P_S G^2 B}\right)^{\frac{v_1}{2}} K_{v_1}\left(2\sqrt{\frac{B\left(\gamma_{th}\text{-}\sigma_2\right)}{\lambda P_S G^2}}\right) \\ &+ Q_4 \left(\frac{\gamma_{th}\text{-}\sigma_2}{\lambda P_S G^2 D}\right)^{\frac{v_2}{2}} K_{v_2}\left(2\sqrt{\frac{D\left(\gamma_{th}\text{-}\sigma_2\right)}{\lambda P_S G^2}}\right), \end{aligned} \tag{14}$$

where Q_i $(i = 1, 2, 3, 4)$ are constants that depend on system and channel parameters. These asymptotic expressions clearly reveal the dependence of detection probabilities on transmit power P_S, channel gains, and RSMA power allocation factors.

B. Outage Probability

According to the RSMA protocol, U_1, after receiving the message from the relay, first decodes the public message x_c while considering the private messages x_1 and x_2 as interference [37]. Subsequently, it performs successive interference cancellation (SIC) to eliminate x_c, and then decodes its own private message streams, considering other users' private message streams as interference. Consequently, the signal-to-interference-plus-noise ratios (SINR) of the received public and private message streams, can be written respectively as

$$\begin{aligned}\gamma_{c1} &= \frac{G^2 P_S P_R \left|h_{SR}\right|^2 h_{u1}^2 \alpha_c}{(\alpha_1+\alpha_2)\, G^2 P_S P_R \left|h_{SR}\right|^2 h_{u1}^2 + G^2 P_R h_{u1}^2 \sigma_1 + \sigma_2} \\ &= \frac{G^2 P_S X Y \alpha_c}{(\alpha_1+\alpha_2)\, G^2 P_S X Y + G^2 Y \sigma_1 + 1}, \end{aligned} \tag{15}$$

$$\gamma_1 = \frac{G^2 P_S X Y \alpha_1}{G^2 Y \sigma_1 + 1}. \tag{16}$$

where h_{u1} represents the channel coefficient associated with U_1. According to the RSMA protocol, when an outage occurs during the transmission of an RSMA user's private and public messages, the outage probability of U_1 can be expressed as

$$\begin{aligned} P_{out} &= 1 - \Pr\left(\gamma_c > \gamma_{\text{thc}}, \gamma_1 > \gamma_{\text{th1}}\right) \\ &= \Pr\left(\gamma_c < \gamma_{\text{thc}}\right) + \Pr\left(\gamma_1 < \gamma_{\text{th1}}\right) \\ &\quad - \Pr\left(\gamma_c < \gamma_{\text{thc}}, \gamma_1 < \gamma_{\text{th1}}\right) \\ &= P_{out}^{c1} + P_{out}^{1} - \Pr\left(\gamma_c < \gamma_{\text{thc}}, \gamma_1 < \gamma_{\text{th1}}\right), \end{aligned} \tag{17}$$

where γ_{thc} and γ_{th1} represent the threshold SINRs for the common and private messages, respectively. From [38], it is known that $\Pr\left(\gamma_c < \gamma_{\text{thc}}, \gamma_1 < \gamma_{\text{th1}}\right) = \min\left\{\Pr\left(\gamma_c < \gamma_{\text{thc}}\right), \Pr\left(\gamma_1 < \gamma_{\text{th1}}\right)\right\}$, and by using the PDFs of X, Y and [36, Eq. (3.471.9)], we can derive the expressions of P_{out}^{c1} and P_{out}^{1}, as shown at the bottom of the next page.

Remark 3: At high SNR, using [34, Eq. (50)] and [36, Eq. (3.471.9)], we have

$$\begin{aligned} P_{out}^{c1,Asy} &\to 1 - e^{-\frac{\sigma_1 \gamma_{\text{thc}}}{P_S \lambda \left[\alpha_c - (\alpha_1+\alpha_2)\gamma_{\text{thc}}\right]}} \frac{1}{\Gamma(\mu)} \left(\frac{\mu}{\bar{\gamma}_u W}\right)^{\mu} \\ &\quad \times \left(\frac{\gamma_{\text{thc}} \bar{\gamma}_u W}{\mu G^2 P_S \lambda \left[\alpha_c - (\alpha_1+\alpha_2)\gamma_{\text{thc}}\right]}\right)^{\frac{\mu}{2}} \\ &\quad \times K_{\mu}\left(\sqrt{\frac{\gamma_{\text{thc}} \mu}{\bar{\gamma}_u W G^2 P_S \lambda \left[\alpha_c - (\alpha_1+\alpha_2)\gamma_{\text{thc}}\right]}}\right), \end{aligned} \tag{20}$$

and

$$\begin{aligned} P_{out}^{1,Asy} &\to 1 - e^{-\frac{\sigma_1 \gamma_{thc1}}{P_S \lambda \alpha_1}} \frac{1}{\Gamma(\mu)} \left(\frac{\mu}{\bar{\gamma}_u W}\right)^{\mu} \\ &\quad \times \left(\frac{\gamma_{\text{th1}} \bar{\gamma}_u W}{\mu G^2 P_S \lambda \alpha_1}\right)^{\frac{\mu}{2}} K_{\mu}\left(\sqrt{\frac{\gamma_{\text{th1}} \mu}{\bar{\gamma}_u W G^2 P_S \lambda \alpha_1}}\right), \end{aligned} \tag{21}$$

based on the above analytical results, the OP has a more concise form $P_{out} \to (G_c \times \bar{\gamma})^{G_d}$, where G_d is the diversity order and G_c represents the coding gain [39]. assuming $\bar{\gamma}_u = \bar{\gamma}_1 = \bar{\gamma}$, where $\bar{\gamma}_1 = \frac{P_S}{\sigma_1}$. By using [40, Eq. (03.04.26.0009.01)] and [40, Eq. (07.34.06.0040.01)], we have

$$P_{out}^{c1,Asy}, P_{out}^{1,Asy} \to \rho_1 \left(\frac{1}{\bar{\gamma}}\right)^{2\mu+1} + \rho_2 \left(\frac{1}{\bar{\gamma}}\right)^{1}, \tag{22}$$

where ρ_1 and ρ_2 are related constants. It can be seen that the system diversity order can be expressed as $G_d = \min\{1, 2\mu+1\}$.

$$\begin{aligned} P_{FA} &= 1 - \frac{\mu^{-\mu} m^m \kappa^{-\mu} (\mu-1)\, \Gamma(m)}{\Gamma(\mu)\, (\mu\kappa+m)^{m-\mu}} \frac{\mu^2 \kappa (1+\kappa)}{(\mu\kappa+m)\, \bar{\gamma}_u W} \sum_{k_1=0}^{m-1} \sum_{k_2=0}^{m-k_1-1} \frac{(-1)^{k_1+k_2}}{k_1!\, (m-k_1-1)!\, k_2!} \frac{(k_1-m+1)_{k_2}}{\Gamma(k_1+k_2+1)} \\ &\times \left[\Gamma(k_1+\mu-1) \left(\frac{\mu^2\kappa(1+\kappa)}{(\mu\kappa+m)\, \bar{\gamma}_u W}\right)^{k_2} k_2!\, B^{-v_1} \left(1 - \sum_{s_1=0}^{k_2} \frac{2}{s_1!} \left(\frac{B(\gamma_{\text{th}}-\sigma_2)\lambda}{\sigma_2 P_S G^2 (\alpha_c+\alpha_2)}\right)^{\frac{1+s_1}{2}} \right.\right. \\ &\times K_{1-s_1}\left(2\sqrt{\frac{B(\gamma_{\text{th}}-\sigma_2)\lambda}{\sigma_2 P_S G^2 (\alpha_c+\alpha_2)}}\right)\Bigg) - \sum_{k_3=0}^{\mu-k_1-2} \frac{(\mu+k_1-1)!}{k_3!} \left(\frac{\mu^2\kappa(1+\kappa)}{(\mu\kappa+m)\, \bar{\gamma}_u W}\right)^{k_2+k_3} (k_2+k_3)! \\ &\times B^{-v_2} \left(1 - \sum_{s_2=0}^{k_2+k_3} \frac{2}{s_2!} \left(\frac{D(\gamma_{\text{th}}-\sigma_2)\lambda}{\sigma_2 P_S G^2 (\alpha_c+\alpha_2)}\right)^{\frac{1+s_2}{2}} K_{1-s_2}\left(2\sqrt{\frac{D(\gamma_{\text{th}}-\sigma_2)\lambda}{\sigma_2 P_S G^2 (\alpha_c+\alpha_2)}}\right)\right)\Bigg]. \end{aligned} \tag{9}$$

$$\begin{aligned} P_{MD} &= \frac{\mu^{-\mu} m^m \kappa^{-\mu} (\mu-1)\, \Gamma(m)}{\Gamma(\mu)\, (\mu\kappa+m)^{m-\mu}} \frac{\mu^2 \kappa (1+\kappa)}{(\mu\kappa+m)\, \bar{\gamma}_u W} \sum_{k_1=0}^{m-1} \sum_{k_2=0}^{m-k_1-1} \frac{(-1)^{k_1+k_2}}{k_1!\, (m-k_1-1)!\, k_2!} \frac{(k_1-m+1)_{k_2}}{\Gamma(k_1+k_2+1)} \\ &\times \left[\Gamma(k_1+\mu-1) \left(\frac{\mu^2\kappa(1+\kappa)}{(\mu\kappa+m)\, \bar{\gamma}_u W}\right)^{k_2} k_2!\, B^{-v_1} \left(1 - \sum_{s_1=0}^{k_2} \frac{2}{s_1!} \left(\frac{B(\gamma_{\text{th}}-\sigma_2)\lambda}{\sigma_2 P_S G^2}\right)^{\frac{1+s_1}{2}} \right.\right. \\ &\times K_{1-s_1}\left(2\sqrt{\frac{B(\gamma_{\text{th}}-\sigma_2)\lambda}{\sigma_2 P_S G^2}}\right)\Bigg) - \sum_{k_3=0}^{\mu-k_1-2} \frac{(\mu+k_1-1)!}{k_3!} \left(\frac{\mu^2\kappa(1+\kappa)}{(\mu\kappa+m)\, \bar{\gamma}_u W}\right)^{k_2+k_3} (k_2+k_3)! \\ &\times B^{-v_2} \left(1 - \sum_{s_2=0}^{k_2+k_3} \frac{2}{s_2!} \left(\frac{D(\gamma_{\text{th}}-\sigma_2)\lambda}{\sigma_2 P_S G^2}\right)^{\frac{1+s_2}{2}} K_{1-s_2}\left(2\sqrt{\frac{D(\gamma_{\text{th}}-\sigma_2)\lambda}{\sigma_2 P_S G^2}}\right)\right)\Bigg]. \end{aligned} \tag{10}$$

C. Covert Transmission Rate

The covert transmission rate C_R is another important indicator of a covert communication system. The significance of the covert transmission rate is that it directly reflects not only the transmission rate that can be achieved by the system without outage, but also the ability of the system to guarantee the communication performance of the legitimate party under the requirement of a covert communication.

The transmission rates at which U_1 decodes its own public information stream x_c and private information stream x_1 can be written as $R_{c1} = \mathbb{E}[\log_2(1+\gamma_{c1})]$ and $R_1 = \mathbb{E}[\log_2(1+\gamma_1)]$ [41], respectively. According to the RSMA protocol, to ensure that each RSMA user can decode the public information stream, the rate for transmitting the complete public information is given by $R_c = \min(R_{c1}, R_{c2})$. In addition, U_1 and U_2 share the transmission rate of all public information. Assuming that the public transmission rates of U_1 and U_2 are C_{c1} and C_{c2}, respectively, we get $C_{c1} + C_{c2} = R_c$. Based on the above analysis, the covert transmission rate of the system can be written as

$$\begin{aligned} C_R &= C_{c1} + R_1 \\ &= \beta R_c + R_1, \end{aligned} \tag{23}$$

where β is the coefficient of the rate distribution satisfying $0 < \beta < 1$.

We note that the exact analysis for (23) is challenging, and calculating its lower bound can be a viable alternative. According to [42, Eq. (30)] and (23), the lower bound for $R_c = \mathbb{E}(\log_2(1+\gamma_c))$ is given by

$$R_c \geq \log_2(1+\exp(\mathbb{E}(\ln\gamma_c))), \tag{24}$$

where $\gamma_c = \min\{\gamma_{c1}, \gamma_{c2}\}$. In particular, $\mathbb{E}(\ln\gamma_c)$ can be rewritten as

$$\begin{aligned} \mathbb{E}(\ln\gamma_c) &= \mathbb{E}\left(\ln G^2 P_S \alpha_c\right) + \mathbb{E}(\ln X) + \mathbb{E}(\ln Y) \\ &\quad - \mathbb{E}\left(\ln\left[(\alpha_1+\alpha_2) G^2 P_S XY + G^2 Y \sigma_1 + 1\right]\right) \\ &= I_1^c + I_2^c + I_3^c - I_4^c, \end{aligned} \tag{25}$$

where

$$I_1^c = \ln\left(G^2 P_S \alpha_c\right). \tag{26}$$

Also, using [36, Eq. (4.331.1)], we can obtain

$$I_2^c = \ln(\lambda), \tag{27}$$

particularly, utilizing [36, Eq. (4.352.1)], [40, Eq. (01.04.26.0003.01)] and [40, Eq. (07.34.21.0088.01)], we can derive I_3^c and I_4^c, as shown at the bottom of the next page, respectively, where $G_{:,:}^{:,:}[\cdot]$ denotes the Meijer's G function.

Proof: See Appendix B.

Similarly, by using (16) and (24), we can obtain

$$R_1 = \mathbb{E}(\log_2(1+\gamma_1)) \geq \log_2(1+\exp(\mathbb{E}(\ln\gamma_1))), \tag{30}$$

where $\mathbb{E}(\ln\gamma_1)$ can be rewritten as

$$\begin{aligned} \mathbb{E}(\ln\gamma_1) &= \mathbb{E}\left(\ln G^2 P_S \alpha_1\right) + \mathbb{E}(\ln X) + \mathbb{E}(\ln Y) \\ &\quad - \mathbb{E}\left(\ln G^2 Y \sigma_1 + 1\right) \\ &= I_1^1 + I_2^1 + I_3^1 - I_4^1, \end{aligned} \tag{31}$$

with I_1^1 given by

$$I_1^1 = \ln\left(G^2 P_S \alpha_1\right), \tag{32}$$

$I_2^1 = I_2^c, I_3^1 = I_3^c$. Finally, after using [40, Eq. (01.04.26.0003.01)] and [40, Eq. (07.34.21.0088.01)], we can derive I_4^1, as shown at the bottom of the next page.

$$\begin{aligned} P_{out}^{c1} &= 1 - \frac{\mu^{-\mu} m^m \kappa^{-\mu}(\mu-1)\Gamma(m)}{\Gamma(\mu)(\mu\kappa+m)^{m-\mu}} \frac{\mu^2\kappa(1+\kappa)}{(\mu\kappa+m)\bar{\gamma}_u W} \sum_{k_1=0}^{m-1}\sum_{k_2=0}^{m-k_1-1} \frac{(-1)^{k_1+k_2}}{(m-k_1-1)!k_1!k_2!} \frac{(k_1-m+1)_{k_2}}{\Gamma(k_1+k_2+1)} \\ &\times 2\exp\left(-\frac{\sigma_1\gamma_{\text{thc}}}{P_S\lambda[\alpha_c-(\alpha_1+\alpha_2)\gamma_{\text{thc}}]}\right)\left[\Gamma(k_1+\mu-1)\left(\frac{\mu^2\kappa(1+\kappa)}{(\mu\kappa+m)\bar{\gamma}_u W}\right)^{k_2}\left(\frac{\gamma_{\text{thc}}}{G^2 B P_S\lambda}\right)^{\frac{v_1}{2}}\right. \\ &\times \left(\frac{1}{[\alpha_c-(\alpha_1+\alpha_2)\gamma_{\text{thc}}]}\right)^{\frac{v_1}{2}} K_{v_1}\left(\sqrt{\frac{\gamma_{\text{thc}} B}{G^2 P_S\lambda[\alpha_c-(\alpha_1+\alpha_2)\gamma_{\text{thc}}]}}\right) - \sum_{k_3=0}^{\mu-k_1-2}\frac{(\mu+k_1-1)!}{k_3!} \\ &\times \left.\left(\frac{\mu^2\kappa(1+\kappa)}{(\mu\kappa+m)\bar{\gamma}_u W}\right)^{k_2+k_3}\left(\frac{\gamma_{\text{thc}}}{G^2 D P_S\lambda[\alpha_c-(\alpha_1+\alpha_2)\gamma_{\text{thc}}]}\right)^{\frac{v_2}{2}} K_{v_2}\left(\sqrt{\frac{\gamma_{\text{thc}} D}{G^2 P_S\lambda[\alpha_c-(\alpha_1+\alpha_2)\gamma_{\text{thc}}]}}\right)\right]. \end{aligned} \tag{18}$$

$$\begin{aligned} P_{out}^{1} &= 1 - \frac{\mu^{-\mu} m^m \kappa^{-\mu}(\mu-1)\Gamma(m)}{\Gamma(\mu)(\mu\kappa+m)^{m-\mu}} \frac{\mu^2\kappa(1+\kappa)}{(\mu\kappa+m)\bar{\gamma}_u W} \sum_{k_1=0}^{m-1}\sum_{k_2=0}^{m-k_1-1} \frac{(-1)^{k_1+k_2}}{(m-k_1-1)!k_1!k_2!} \frac{(k_1-m+1)_{k_2}}{\Gamma(k_1+k_2+1)} \\ &\times 2\exp\left(-\frac{\sigma_1\gamma_{\text{th}1}}{P_S\lambda\alpha_1}\right)\left[\Gamma(k_1+\mu-1)\left(\frac{\mu^2\kappa(1+\kappa)}{(\mu\kappa+m)\bar{\gamma}_u W}\right)^{k_2}\left(\frac{\gamma_{\text{th}1}}{G^2 B P_S\lambda\alpha_1}\right)^{\frac{v_1}{2}} K_{v_1}\left(\sqrt{\frac{\gamma_{\text{th}1} B}{G^2 P_S\lambda\alpha_1}}\right)\right. \\ &\left. - \sum_{k_3=0}^{\mu-k_1-2}\frac{(\mu+k_1-1)!}{k_3!}\left(\frac{\mu^2\kappa(1+\kappa)}{(\mu\kappa+m)\bar{\gamma}_u W}\right)^{k_2+k_3}\left(\frac{\gamma_{\text{th}1}}{G^2 D P_S\lambda\alpha_1}\right)^{\frac{v_2}{2}} K_{v_2}\left(\sqrt{\frac{\gamma_{th} D}{G^2 P_S\lambda\alpha_1}}\right)\right]. \end{aligned} \tag{19}$$

The preceding performance analysis assumes integer values for fading parameters m and μ for simplicity. However, practical underwater environments often involve real-valued parameters. Next section extends the analysis to this general case, enhancing the applicability of our theoretical results.

IV. Extension to Arbitrary Real-Valued m and μ

To provide more general results, we extend the OP analysis to the case where the fading parameters m and μ take arbitrary positive real values. Based on the general form of the PDF for the UAC link presented in [34, Eq. (5)], and by employing the confluent hypergeometric series expansion given in [40, Eq. (07.20.06.0003.02)] ${}_1F_1(a;b;z) = \sum_{k=0}^{\infty} \frac{(a)_k}{(b)_k} \frac{z^k}{k!}$, where ${}_1F_1(\cdot;\cdot;\cdot)$ denotes the confluent hypergeometric function of the first kind, we have

$$f_y^{\kappa-\mu}(y) = \frac{\mu^{\mu} m^{m} (1+\kappa)^{\mu}}{\Gamma(\mu)\,\bar{\gamma}_u W\,(\mu\kappa+m)^{m}} \left(\frac{y}{\bar{\gamma}_u W}\right)^{\mu-1} \times \exp\left(-\frac{\mu(1+\kappa)y}{\bar{\gamma}_u W}\right) \sum_{k=0}^{\infty} \frac{(m)_k}{(\mu)_k\, k!} \left(\frac{\mu^2\kappa(1+\kappa)}{\mu\kappa+m}\frac{y}{\bar{\gamma}_u W}\right)^{k}, \tag{34}$$

and utilizing the PDFs of X and Y, along with integral identities from [36, Eq. (3.471.9)] $\bar{P}_{out}^{c1}$ can be expressed as

$$\bar{P}_{out}^{c1} = 1 - \sum_{k=0}^{\infty} \frac{2\mu^{\mu} m^{m} (1+\kappa)^{\mu}}{\Gamma(\mu)(\mu\kappa+m)^{m}(\bar{\gamma}_u W)^{\mu}} \frac{(m)_k}{(\mu)_k k!} \times \left(\frac{\mu^2\kappa(1+\kappa)}{(\mu\kappa+m)\bar{\gamma}_u W}\right)^{k} \left(\frac{\gamma_{\text{thc}}\bar{\gamma}_u W}{P_S\mu\lambda(1+\kappa)[\alpha_c-\gamma_{\text{thc}}(\alpha_1+\alpha_2)]}\right)^{\frac{k+\mu}{2}} \times K_{k+\mu}\left(2\sqrt{\frac{\gamma_{\text{thc}}\mu\lambda(1+\kappa)}{P_S\bar{\gamma}_u W[\alpha_c-\gamma_{\text{thc}}(\alpha_1+\alpha_2)]}}\right), \tag{35}$$

this new expression removes the restriction that m and μ must be integers, thus enabling the performance evaluation of covert communication systems over generalized $\kappa-\mu$ shadowed UAC fading channels with arbitrary real-valued fading parameters.

V. Numerical Results and Discussion

To validate the theoretical derivations for both the base case and the extended scenario, this section presents numerical simulations. These results confirm the accuracy of the analytical expressions and demonstrate the impact of key parameters on system performance.

To ensure statistical reliability, the number of Monte Carlo iterations is set to 10^6. Unless stated otherwise, the default simulation parameters include the $\kappa-\mu$ shadowed fading

$$I_3^c = \frac{\mu^{-\mu} m^m \kappa^{-\mu} (\mu-1)\Gamma(m)}{\Gamma(\mu)(\mu\kappa+m)^{m-\mu}} \frac{\mu^2\kappa(1+\kappa)}{(\mu\kappa+m)\bar{\gamma}_u W} \sum_{k_1=0}^{m-1}\sum_{k_2=0}^{m-k_1-1} \frac{(-1)^{k_1+k_2}}{k_1!(m-k_1-1)!k_2!} \frac{(k_1-m+1)_{k_2}}{\Gamma(k_1+k_2+1)} \times \Bigg[\Gamma(k_1+\mu-1)\left(\frac{\mu^2\kappa(1+\kappa)}{(\mu\kappa+m)\bar{\gamma}_u W}\right)^{k_2} B^{-v_1}\Gamma(v_1)(\psi(v_1)-\ln B) - \sum_{k_3=0}^{\mu-k_1-2}\frac{(\mu+k_1-1)!}{k_3!}\left(\frac{\mu^2\kappa(1+\kappa)}{(\mu\kappa+m)\bar{\gamma}_u W}\right)^{k_2+k_3} D^{-v_2}\Gamma(v_2)(\psi(v_2)-\ln D)\Bigg]. \tag{28}$$

$$I_4^c = \frac{\mu^{-\mu} m^m \kappa^{-\mu} (\mu-1)\Gamma(m)}{\Gamma(\mu)(\mu\kappa+m)^{m-\mu}} \frac{\mu^2\kappa(1+\kappa)}{(\mu\kappa+m)\bar{\gamma}_u W} \sum_{k_1=0}^{m-1}\sum_{k_2=0}^{m-k_1-1} \frac{(-1)^{k_1+k_2}}{k_1!(m-k_1-1)!k_2!} \frac{(k_1-m+1)_{k_2}}{\Gamma(k_1+k_2+1)} \times \Bigg[\Gamma(k_1+\mu-1)\left(\frac{\mu^2\kappa(1+\kappa)}{(\mu\kappa+m)\bar{\gamma}_u W}\right)^{k_2} B^{-v_1} \mathrm{G}_{4,2}^{1,4}\left[\frac{G^2 P_S\lambda(\alpha_1+\alpha_2)}{B}\middle|\begin{matrix}-k_2,1,1,0\\1,0\end{matrix}\right] - \sum_{k_3=0}^{\mu-k_1-2}\frac{(\mu+k_1-1)!}{k_3!}\left(\frac{\mu^2\kappa(1+\kappa)}{(\mu\kappa+m)\bar{\gamma}_u W}\right)^{k_2+k_3} D^{-v_2} \mathrm{G}_{4,2}^{1,4}\left[\frac{G^2 P_S\lambda(\alpha_1+\alpha_2)}{D}\middle|\begin{matrix}-k_2-k_3,1,1,0\\1,0\end{matrix}\right]\Bigg] \tag{29}$$

$$I_4^1 = \frac{\mu^{-\mu} m^m \kappa^{-\mu} (\mu-1)\Gamma(m)}{\Gamma(\mu)(\mu\kappa+m)^{m-\mu}} \frac{\mu^2\kappa(1+\kappa)}{(\mu\kappa+m)\bar{\gamma}_u W} \sum_{k_1=0}^{m-1}\sum_{k_2=0}^{m-k_1-1} \frac{(-1)^{k_1+k_2}}{k_1!(m-k_1-1)!k_2!} \frac{(k_1-m+1)_{k_2}}{\Gamma(k_1+k_2+1)} \times \Bigg[\Gamma(k_1+\mu-1)\left(\frac{\mu^2\kappa(1+\kappa)}{(\mu\kappa+m)\bar{\gamma}_u W}\right)^{k_2} B^{-v_1} \mathrm{G}_{3,2}^{1,3}\left[\frac{G^2\sigma_1}{B}\middle|\begin{matrix}-k_2,1,1,\\1,0\end{matrix}\right] - \sum_{k_3=0}^{\mu-k_1-2}\frac{(\mu+k_1-1)!}{k_3!}\left(\frac{\mu^2\kappa(1+\kappa)}{(\mu\kappa+m)\bar{\gamma}_u W}\right)^{k_2+k_3} D^{-v_2} \mathrm{G}_{3,2}^{1,3}\left[\frac{G^2\sigma_1}{D}\middle|\begin{matrix}-k_2-k_3,1,1,\\1,0\end{matrix}\right]\Bigg] \tag{33}$$

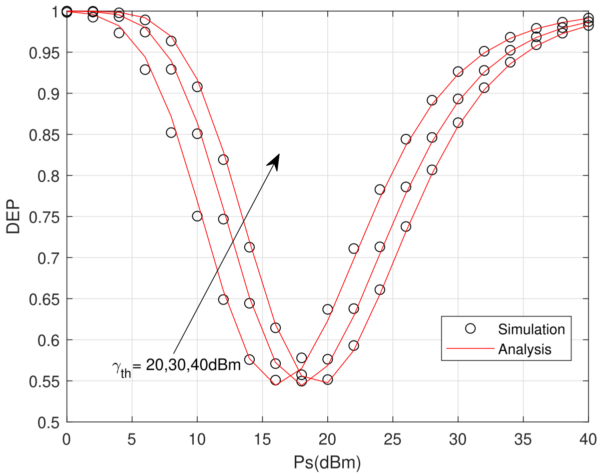

Fig. 2. The DEP for different values of γ_{th}.

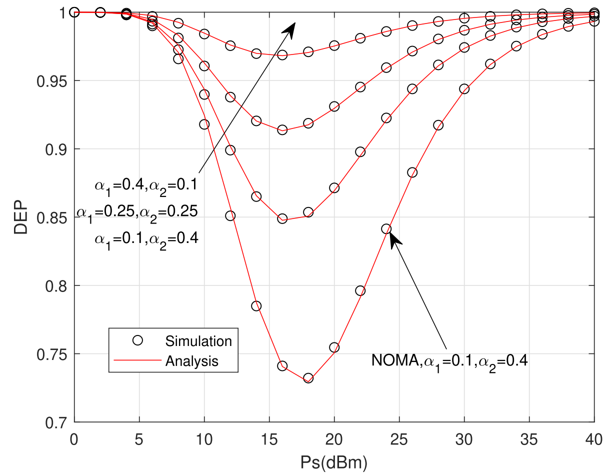

Fig. 3. The DEP for different values of α_1 and α_2.

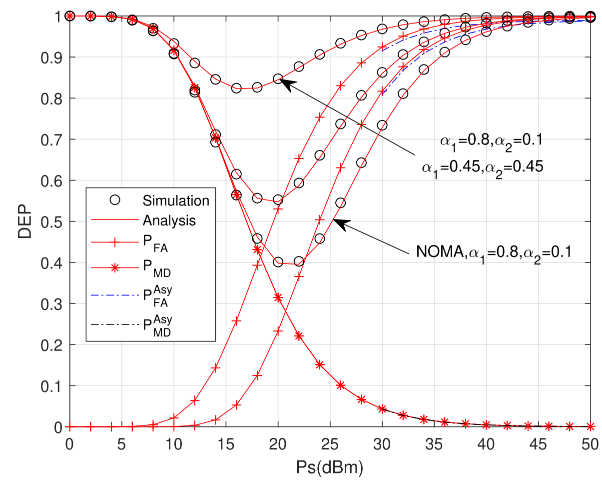

Fig. 4. The DEP, P_{FA}, and P_{MD} trend for different values of α_1 and α_2.

parameters κ=5, μ=2, m=3, the underwater path loss factor W=1, noise variances σ_1=σ_2=-5 dBm, the SINR thresholds γ_{th}=$\gamma_{\text{th}1}$=$\gamma_{\text{th}c}$=0.1 dBm, and amplification gain G=1.5. The transmit power levels and power allocation factors are set to α_c=0.1, α_1=0.8, α_2=0.1, and the RSMA-related parameter β is set to 0.5. The inverse fading mean is denoted by λ=1/$\mathbb{E}(X)$. It can be observed that the theoretical and Monte Carlo results match well, validating the accuracy of our analysis under diverse operating conditions.

Fig. 2 illustrates the variation of the DEP in a covert communication system with changes in the SNR threshold. Specifically, as the SNR threshold increases, the minimum point of DEP shifts to the right. This indicates that as the SNR increases, it becomes easier for the covert communication system to differentiate between the signal and noise, making the detection of the covert signal more challenging. Consequently, the communication system ability to remain undetected improves. This trend is particularly important in covert communications, where the core objective is to prevent detection by eavesdroppers. A higher SNR allows the system to operate with stronger signals, reducing the likelihood of false detection and enhancing the system's covert nature.

Fig. 3 presents the DEP under varying values of α_1 and α_2, with the public stream α_c held constant. As α_1 increases, the DEP minimum point shifts upward. The increasing α_1 represents a greater allocation of resources to U_1 private stream, which in turn enhances the signal power of U_1. However, this increased allocation results in higher detectability of the covert signal, which leads to a rise in the DEP. This behavior highlights the trade-off between improving communication quality for the legitimate user and maintaining the covert nature of the communication. As the power of U_1 private stream (α_1) increases, the system becomes more susceptible to detection, thus shifting the DEP curve upward. This suggests that while the system benefits from a higher α_1 in terms of communication quality, it loses some of its ability to hide the signal effectively. In addition, a baseline NOMA configuration (α_1=0.1, α_2=0.4) is also plotted in Fig. 3 for comparison purposes. It can be observed that the DEP of NOMA is generally lower than that of RSMA, indicating a higher likelihood of being detected. This result implies that RSMA, through a flexible message splitting and power allocation, is more capable of enhancing the covert performance under the same total power constraints.

Fig. 4 presents the relationship between the DEP, P_{FA}, and P_{MD} under different α_1 and α_2 values, with a public stream α_c fixed. As α_1 increases, the minimum point of the DEP shifts downward, which indicates that the covert communication system becomes more robust against detection as more resources are allocated to U_1 private stream. Furthermore, P_{MD} shows a minimal variation, suggesting that the system ability to avoid a missed detection remains stable across the changes in α_1. This characteristic is critical for maintaining a reliable covert communication system, as a missed detection could lead to a failure in concealing the transmission. On the other hand, P_{FA} shifts slightly to the right, indicating that the system becomes less likely to generate false alarms as α_1 increases. A reduced P_{FA} is desirable for covert communication, as it minimizes the risk of raising suspicions by false detection of signals. The results indicate that by adjusting α_1, the system can be tuned to reduce both DEP and P_{FA}, while maintaining a stable P_{MD}. This

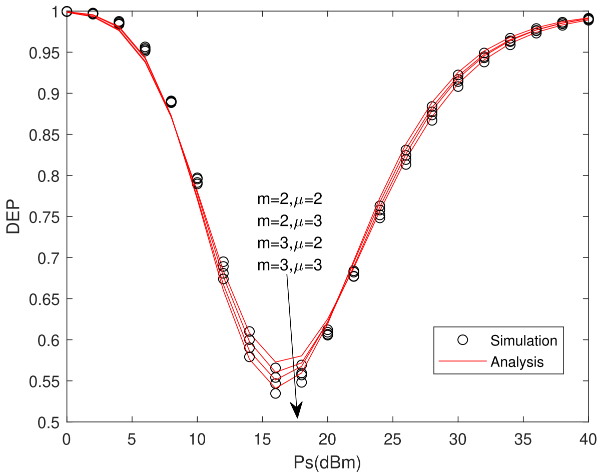

Fig. 5. The DEP performance for different values of m and μ.

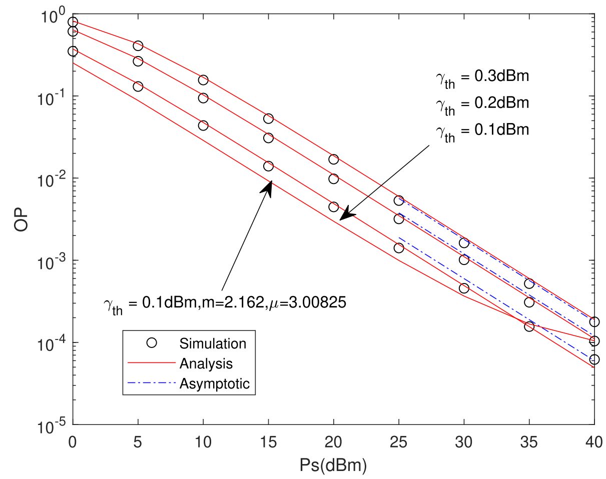

Fig. 6. The OP performance for different values of γ_{th}.

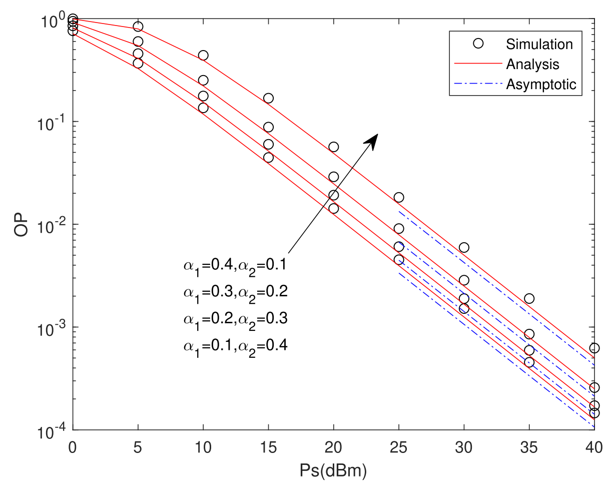

Fig. 7. The OP for different values of α_1 and α_2.

optimization highlights the importance of resource allocation in improving covert communication performance. In addition, a NOMA-based baseline configuration is plotted in Fig. 1 to serve as benchmark. The asymptotic curves for P_{FA} and P_{MD} are also plotted and show excellent agreement with simulation results in the high-SNR region, validating the accuracy of our approximations.

In Fig. 5, we explore the impact of the UAC link parameters m and μ on the DEP. It is evident that the minimum DEP point shifts downward as the values of m and μ increase. This behavior suggests that variations in the UAC link parameters have a subtle effect on the covert communication system's ability to avoid detection, with larger values of m and μ contributing to improved covertness. The results presented in Figs. 2–5 provide significant insights into the performance of the RSMA-assisted RF-UAC covert communication system. The analyses reveal the intricate relationships between various system parameters such as the SNR threshold, resource allocation (α_1 and α_2), and the characteristics of the UAC link (m and μ). Moreover, the system exhibits a trade-off between communication quality and covert performance, where increasing α_1 can improve the communication quality for legitimate users but also increases the risk of detection. Additionally, the UAC link parameters m and μ play a crucial role in enhancing the system resilience to fading and shadowing, albeit with limited impact on the DEP in high-SNR regimes. These findings underscore the importance of carefully optimizing system parameters to achieve the desired balance between communication reliability and the need for secure, covert transmission in complex environments.

Fig. 6 illustrates the impact of different SNR thresholds γ_{th} on the OP, including the case where the fading parameters m and μ are real-valued. As expected, the OP decreases as the transmit power P_S increases. Moreover, a lower γ_{th} results in a lower OP across all power levels, reflecting that the system can meet lower quality-of-service requirements more easily. Additionally, the plotted results include the case where $m = 2.162$ and $\mu = 3.00825$, demonstrating that the proposed OP expressions are not limited to integer values of fading parameters. The analytical and asymptotic curves remain tightly matched with the simulation data, which confirms the correctness and generality of the derived expressions under arbitrary fading conditions. These findings reinforce the robustness of the proposed theoretical framework and provide important guidelines for system design under realistic channel statistics, particularly when modeling underwater acoustic links with non-integer fading parameters.

Fig. 7 demonstrates that as α_1 increases, the OP begins to decrease rapidly. Specifically, increasing α_1 allocates more resources to U_1, thereby improving the signal strength and reliability of this user. As more resources are assigned to U_1 private stream, the communication quality of U_1 improves, allowing the system to overcome interference and noise impacts earlier. The earlier decrease in the OP means that the system achieves better performance at lower thresholds. Therefore, resource allocation plays a key role in optimizing the outage probability in covert communication systems.

Fig. 8 demonstrates that as α_1 increases, the CR also increases, given a constant public stream α_c. This indicates that when more resources are allocated to the private stream of U_1, the system can transmit information at a higher rate without compromising its ability to remain undetectable. The

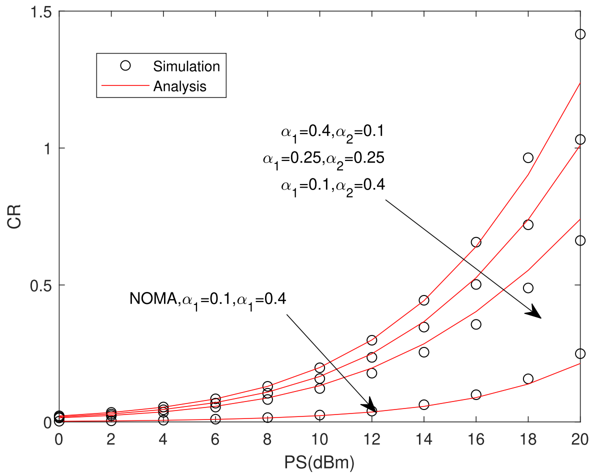

Fig. 8. The CR for different values of α_1 and α_2.

increase in α_1 enhances the communication capacity of the system, leading to a higher CR. This is an important feature for covert communication, where the balance between data rate and concealment is critical. By increasing the private stream allocation (α_1), the system can achieve higher data rates while still maintaining a low probability of detection. The figure also includes a benchmark NOMA curve for comparison purposes. It can be observed that the RSMA-based scheme consistently achieves higher CR values across the entire range of α_1 compared to the NOMA-based one. This is attributed to the RSMA's flexible interference management and its ability to superimpose public and private messages more efficiently, leading to and improved resource utilization. In summary, Figs. 6, 7, and 8 provide insights into how different system parameters, such as SNR thresholds and resource allocation between public and private streams, impact the performance of covert communication. Fig. 6 shows the relationship between SNR thresholds and OP, illustrating the slow decay of the OP at higher SNR levels. Fig. 7 emphasizes the significance of resource allocation, demonstrating how increasing α_1 improves system reliability by reducing the OP. Lastly, Fig. 8 highlights the trade-off between covert communication rate and resource allocation, showing that higher α_1 values lead to an increased CR without compromising covert performance. These results underline the importance of carefully balancing public and private streams to optimize both the reliability and efficiency of covert communication systems.

Fig. 9(a) illustrates the variation of covert transmission rate (CR) with respect to different power allocation factors. In Fig. 9(a), the CR is plotted against α_1 and α_2, while α_c is fixed. It is evident that the CR increases monotonically as α_1 increases and α_2 decreases. This trend highlights that allocating more power to U_1's private stream improves its effective communication rate, while reducing the interference caused by U_2. In RSMA systems, this efficient allocation enhances the overall covert throughput. In Fig. 9(b), the relationship between CR and the power allocation coefficients α_1 and α_c is shown. It is evident that the CR increases with higher values of both α_1 and α_c, indicating that jointly improving the power of U_1's private stream and the common stream benefits

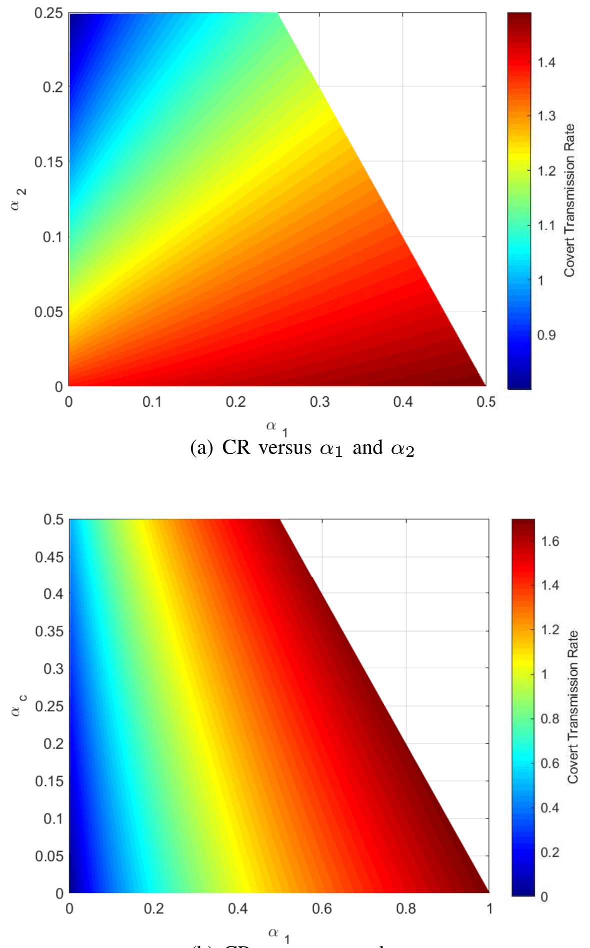

(a) CR versus α_1 and α_2

(b) CR versus α_1 and α_c

Fig. 9. CR versus power distribution factors.

the total covert rate. These results jointly demonstrate that the covert transmission performance in RSMA-based systems can be significantly improved through an appropriate power distribution among private and public streams. Specifically, increasing α_1 and α_c while maintaining a low value of α_2 leads to an optimal CR performance. This observation provides valuable insight for practical resource allocation strategies in covert communication scenarios.

Finally, from a deployment perspective, these metrics jointly inform the trade-offs between covertness, reliability, and data rate. The DEP helps define power control thresholds to maintain a low detectability, the OP guides the resilience strategy under adverse channel conditions, and the CR provides a benchmark for the achievable throughput under covert operation. Together, they serve as essential design references for real-world applications including maritime surveillance, underwater sensor networks, and secure command-and-control of uncrewed platforms.

VI. Conclusion

In this paper, we have proposed and analyzed the covert communication performance of an RSMA-assisted RF-UAC system. The system was modeled as Rayleigh distributed for the RF link and the UAC link followed a $\kappa-\mu$ shadowed distribution. We evaluated key performance metrics such as the DEP, OP, and CR under varying system parameters, including SNR thresholds, and allocation factors α_1, α_2, and α_c for the public and private streams. The analytical results were validated through Monte Carlo simulations, demonstrating the robustness and accuracy of the proposed theoretical framework. To further highlight the effectiveness of the proposed system, we included a baseline NOMA-based scheme for comparison purposes. The results demonstrated that RSMA consistently outperforms NOMA in terms of achievable covert rate and robustness to detection. In conclusion, the RSMA-assisted RF-UAC system offers a promising approach for covert communication in underwater environments, where reliable signal concealment is critical. Future work can explore the integration of advanced interference management techniques and optimization strategies to further enhance the system performance in more complex communication scenarios.

Appendix A
The Proof of P_{FA}

According to (7), P_{FA} can be reformulated as

$$\begin{aligned} P_{FA} &= \Pr\left(H_0 > \gamma_{\text{th}}\right) \\ &= 1-\Pr\left(H_0 < \gamma_{\text{th}}\right) \\ &= 1-\Pr\left(P_S X G^2 Y(\alpha_c+\alpha_2) + G^2 Y \sigma_1 + 1 < \frac{\gamma_{\text{th}}}{\sigma_2}\right) \\ &= 1-\Pr\left(Y < \frac{\gamma_{\text{th}}-\sigma_2}{P_S X G^2 \sigma_2(\alpha_c+\alpha_2) + G^2\sigma_1\sigma_2}\right) \\ &= 1-\int_0^\infty \int_0^{y_1} f_x(x) f_y(y)\,\mathrm{d}y\mathrm{d}x \\ &= 1-T_1, \end{aligned} \tag{36}$$

where $y_1 = \frac{\gamma_{\text{th}}-\sigma_2}{P_S G^2\sigma_2(\alpha_c+\alpha_2)x + G^2\sigma_1\sigma_2}$ and for ease of representation, we assume that $f_y(y) = Ay^{k_2}e^{-By}$, and A, B are constant. By using [36, Eq. (3.351.1)], [36, Eq. (8.352)], T_1 can be rewritten as

$$\begin{aligned} T_1 &= \int_0^\infty f_x(x) \int_0^{y_1} Ay^{k2}e^{-By}\mathrm{d}y\mathrm{d}x \\ &= \int_0^\infty f_x(x) B^{-k_2-1}\Upsilon(k_2+1, y_1)\mathrm{d}x \\ &= \int_0^\infty \frac{e^{-\frac{x}{\lambda}}}{\lambda} B^{-k_2-1}\left(k_2! - k_2! e^{-y_1}\sum_{m=0}^{n}\left(\frac{y_1^m}{m!}\right)\right)\mathrm{d}x. \end{aligned} \tag{37}$$

where $\Upsilon(\cdot,\cdot)$ denotes the generalized incomplete gamma function. Since the integral of the form $(ax+b)^{-m}e^{-\frac{c}{ax+b}-dx}$ is analytically intractable, we consider a high-SNR approximation by substituting $y_1 = \frac{\gamma_{\text{th}}-\sigma_2}{P_S G^2\sigma_2(\alpha_c+\alpha_2)x}$. Using the result from [36, Eq. (3.471.9)], the expression for P_{FA} can then be obtained.

Appendix B
The Proof of I_4^c

According to (25), we have

$$I_4^c = \mathbb{E}\left(\ln\left[(\alpha_1+\alpha_2)G^2 P_S XY + G^2 Y\sigma_1 + 1\right]\right). \tag{38}$$

For ease of representation, we also assume that $f_y(y) = Ay^{k_2}e^{-By}$, and transform $\ln\left[(\alpha_1+\alpha_2)G^2P_SXY + G^2Y\sigma_1+1\right]$ into $\ln(ay+1)$, where $a = (\alpha_1+\alpha_2)G^2P_SX + G^2\sigma_1$, and by utilizing [40, Eq. (01.04.26.0003.01)], [40, Eq. (07.34.21.0088.01)], (38) can be expressed as

$$\begin{aligned} I_4^c &= \int_0^\infty \int_0^\infty f_x(x) f_y(y)\ln(ay+1)\,\mathrm{d}y\mathrm{d}x \\ &= \int_0^\infty f_x(x)\int_0^{y_1} Ay^{k2}e^{-By}\ln(ay+1)\,\mathrm{d}y\mathrm{d}x \\ &= \int_0^\infty f_x(x)\int_0^{y_1} Ay^{k2}e^{-By}\mathrm{G}_{2,2}^{1,2}\left[ay\left|\begin{matrix}1,1,\\1,0\end{matrix}\right.\right]\mathrm{d}y\mathrm{d}x \\ &= \int_0^\infty \frac{e^{-\frac{x}{\lambda}}}{\lambda}AB^{-k_2-1}\mathrm{G}_{3,2}^{1,3}\left[\frac{a}{B}\left|\begin{matrix}-k_2,1,1,\\1,0\end{matrix}\right.\right]\mathrm{d}x \\ &= \int_0^\infty \frac{e^{-\frac{x}{\lambda}}}{\lambda}AB^{-k_2-1}G_1\mathrm{d}x, \end{aligned} \tag{39}$$

where $G_1 = \mathrm{G}_{3,2}^{1,3}\left[\frac{(\alpha_1+\alpha_2)G^2P_Sx+G^2\sigma_1}{B}\left|\begin{matrix}-k_2,1,1,\\1,0\end{matrix}\right.\right]$ is a Meijer's G function with an offset. Considering its high computational complexity and incomplete support on MATLAB, we consider approximation of $a = (\alpha_1+\alpha_2)G^2P_Sx$ under high SNR conditions, and after using [40, Eq. (07.34.21.0088.01)], we can obtain I_4^c.

References

[1] Y. Liu, X. Wang, G. Boudreau, A. B. Sediq, and H. Abou-Zeid, “A multi-dimensional intelligent multiple access technique for 5G beyond and 6G wireless networks,” *IEEE Trans. Wireless Commun.*, vol. 20, no. 2, pp. 1308–1320, Feb. 2021.

[2] Z. Zeng, S. Fu, H. Zhang, Y. Dong, and J. Cheng, “A survey of underwater optical wireless communications,” *IEEE Commun. Surveys Tuts.*, vol. 19, no. 1, pp. 204–238, 1st Quart., 2017.

[3] J. Xiang, L. Yang, K. Guo, N. Zlatanov, and Y. Wu, “Performance evaluation of UAV-aided radio frequency-UAC relaying systems,” *IEEE Internet Things J.*, vol. 11, no. 13, pp. 24183–24195, Jul. 2024.

[4] Z. Xiao, L. Yang, P. S. Bithas, I. S. Ansari, X. Li, and M.-S. Alouini, “Performance analysis of mixed underwater acoustic/optical relaying systems,” *IEEE Trans. Wireless Commun.*, vol. 23, no. 9, pp. 11357–11371, Sep. 2024.

[5] T. Q. Duong, G. C. Alexandropoulos, H.-J. Zepernick, and T. A. Tsiftsis, “Orthogonal space–time block codes with CSI-assisted amplify-and-forward relaying in correlated Nakagami-*m* fading channels,” *IEEE Trans. Veh. Technol.*, vol. 60, no. 3, pp. 882–889, Mar. 2011.

[6] B. Pranitha and L. Anjaneyulu, “Review of research trends in underwater communications—A technical survey,” in *Proc. Int. Conf. Commun. Signal Process. (ICCSP)*, Apr. 2016, pp. 1443–1447.

[7] P. Kumar, V. K. Trivedi, and P. Kumar, “Recent trends in multicarrier underwater acoustic communications,” in *Proc. IEEE Underwater Technol. (UT)*, Feb. 2015, pp. 1–8.

[8] H. Kaushal and G. Kaddoum, “Underwater optical wireless communication,” *IEEE Access*, vol. 4, pp. 1518–1547, 2016.

[9] K. W. S. Palitharathna, R. I. Godaliyadda, V. R. Herath, and H. A. Suraweera, “Relay-assisted optical wireless communications in turbid water,” in *Proc. 13th ACM Int. Conf. Underwater Netw. Syst.*, Dec. 2018, pp. 1–5.

[10] H. Nam and S. An, “An ultrasonic sensor based low-power acoustic modem for underwater communication in underwater wireless sensor networks,” in *Proc. Int. Conf. Embedded Ubiquitous Comput.*, 2007, pp. 494–504.

[11] K. P. Peppas, G. C. Alexandropoulos, C. K. Datsikas, and F. I. Lazarakis, “Multivariate gamma–gamma distribution with exponential correlation and its applications in radio frequency and optical wireless communications,” *IET Microw., Antennas Propag.*, vol. 5, no. 3, pp. 364–371, Feb. 2011.

[12] W.-B. Yang and T. C. Yang, "High-frequency channel characterization for M-ary frequency-shift-keying underwater acoustic communications," *J. Acoust. Soc. Amer.*, vol. 120, no. 5, pp. 2615–2626, Nov. 2006.

[13] J. F. Paris, "Statistical characterization of κ—μ shadowed fading," *IEEE Trans. Veh. Technol.*, vol. 63, no. 2, pp. 518–526, Feb. 2014.

[14] K. P. Peppas, G. C. Alexandropoulos, and P. T. Mathiopoulos, "Performance analysis of dual-hop AF relaying systems over mixed η-μ and κ–μ fading channels," *IEEE Trans. Veh. Technol.*, vol. 62, no. 7, pp. 3149–3163, Sep. 2013.

[15] O. S. Badarneh, "The α-F composite fading distribution: Statistical characterization and applications," *IEEE Trans. Veh. Technol.*, vol. 69, no. 8, pp. 8097–8106, Aug. 2020.

[16] K. P. Peppas, G. C. Alexandropoulos, P. T. Mathiopoulos, and J. Yang, "On the sum of ordered random variables and its applications to physical-layer security of communication over η-μ fading channels with generalized selection combining," *Trans. Emerg. Telecommun. Technol.*, vol. 29, no. 6, Jun. 2018, Art. no. e3264.

[17] A. Mukherjee, S. A. A. Fakoorian, J. Huang, and A. L. Swindlehurst, "Principles of physical layer security in multiuser wireless networks: A survey," *IEEE Commun. Surveys Tuts.*, vol. 16, no. 3, pp. 1550–1573, 3rd Quart., 2014.

[18] Y. Zou, J. Zhu, X. Wang, and L. Hanzo, "A survey on wireless security: Technical challenges, recent advances, and future trends," *Proc. IEEE*, vol. 104, no. 9, pp. 1727–1765, Sep. 2016.

[19] Y. Su, H. Sun, Z. Zhang, Z. Lian, Z. Xie, and Y. Wang, "Covert communication with relay selection," *IEEE Wireless Commun. Lett.*, vol. 10, no. 2, pp. 421–425, Feb. 2021.

[20] J. A. de Carvalho, D. B. da Costa, L. Yang, G. C. Alexandropoulos, R. Oliveira, and U. S. Dias, "User fairness in wireless powered communication networks with non-orthogonal multiple access," *IEEE Wireless Commun. Lett.*, vol. 10, no. 1, pp. 189–193, Jan. 2021.

[21] S. Han, H. Xia, X. Zhou, and C. Li, "Securing RSMA-based communications at physical layer," *IEEE Netw.*, vol. 38, no. 2, pp. 211–217, Mar. 2024.

[22] X. Liu, J. Feng, F. Li, and V. C. M. Leung, "Downlink energy efficiency maximization for RSMA-UAV assisted communications," *IEEE Wireless Commun. Lett.*, vol. 13, no. 1, pp. 98–102, Jan. 2024.

[23] S. K. Singh, K. Agrawal, K. Singh, and C.-P. Li, "Ergodic capacity and placement optimization for RSMA-enabled UAV-assisted communication," *IEEE Syst. J.*, vol. 17, no. 2, pp. 2586–2589, Jun. 2023.

[24] Y. Zhang et al., "Rate-splitting multiple access for covert communications," *IEEE Wireless Commun. Lett.*, vol. 13, no. 6, pp. 1685–1689, Jun. 2024.

[25] T. T. Nguyen, N. C. Luong, S. Feng, K. Elbassioni, and D. Niyato, "Jamming-based covert communication for rate-splitting multiple access," *IEEE Trans. Veh. Technol.*, vol. 72, no. 8, pp. 11074–11079, Aug. 2023.

[26] Y. Liang, L. Yang, I. Ahmad, and M. Valkama, "Covert transmission and physical-layer security of STAR-RIS-assisted uplink SGF-NOMA systems," *IEEE Trans. Commun.*, p. 1, 2025, doi: 10.1109/TCOMM.2025.3565500.

[27] Z. Zhang, L. Yang, H. Lei, X. Li, and D. Niyato, "Covert communication in RSMA-assisted ambient backscatter communication systems," *IEEE Trans. Wireless Commun.*, vol. 24, no. 8, pp. 6566–6579, Aug. 2025, doi: 10.1109/TWC.2025.3554667.

[28] Z. Rahman, M. Z. Hassan, and G. Kaddoum, "Ergodic capacity optimization for RSMA-based UOWC systems over EGG turbulence channel," *IEEE Commun. Lett.*, vol. 28, no. 3, pp. 587–591, Mar. 2024.

[29] J. Chen, J. Wang, Z. Wei, Y. Ren, C. Masouros, and Z. Han, "Joint autonomous underwater vehicle trajectory and energy optimization for underwater covert communications," *IEEE Trans. Commun.*, vol. 72, no. 11, pp. 7327–7341, Nov. 2024.

[30] S. Huang, X. Hou, W. Liu, G. Liu, Y. Dai, and W. Tian, "Mimicking ship-radiated noise with chaos signal for covert underwater acoustic communication," *IEEE Access*, vol. 8, pp. 180341–180351, 2020.

[31] C. Gao, B. Yang, D. Zheng, X. Jiang, and T. Taleb, "Cooperative jamming and relay selection for covert communications in wireless relay systems," *IEEE Trans. Commun.*, vol. 72, no. 2, pp. 1020–1032, Feb. 2024.

[32] G. Fang, J. Chen, G. Li, R. He, H. Wang, and Y. Yang, "Joint power allocation for transmitter and relay in a full-duplex relay covert communication system," *IEEE Open J. Commun. Soc.*, vol. 5, pp. 6674–6685, 2024.

[33] X. Li et al., "Covert communication of STAR-RIS aided NOMA networks," *IEEE Trans. Veh. Technol.*, vol. 73, no. 6, pp. 9055–9060, Jun. 2024.

[34] L. Yang et al., "Performance analysis of relay-aided satellite-underwater acoustic communication systems," *IEEE Trans. Commun.*, vol. 72, no. 6, pp. 3511–3525, Jun. 2024.

[35] L. Lv, Q. Wu, Z. Li, Z. Ding, N. Al-Dhahir, and J. Chen, "Covert communication in intelligent reflecting surface-assisted NOMA systems: Design, analysis, and optimization," *IEEE Trans. Wireless Commun.*, vol. 21, no. 3, pp. 1735–1750, Mar. 2022.

[36] I. S. Gradshteyn and I. M. Ryzhic, *Table of Integrals, Series, and Products*, 7th ed., San Diego, CA, USA: Academic, 2007.

[37] Y. Mao, B. Clerckx, and V. O. K. Li, "Rate-splitting multiple access for downlink communication systems: Bridging, generalizing, and outperforming SDMA and NOMA," *EURASIP J. Wireless Commun. Netw.*, vol. 2018, no. 1, pp. 1–54, Dec. 2018.

[38] Y. Zhang, Z. Xiao, L. Yang, P. S. Bithas, M. O. Hasna, and G. K. Karagiannidis, "Mixed RF/FSO communication systems with rate splitting," *IEEE J. Sel. Areas Commun.*, vol. 43, no. 5, pp. 1621–1634, May 2025.

[39] Z. Wang and G. B. Giannakis, "A simple and general parameterization quantifying performance in fading channels," *IEEE Trans. Commun.*, vol. 51, no. 8, pp. 1389–1398, Aug. 2003.

[40] *The Wolfram Functions Site*. [Online]. Available: https://functions.wolfram.com

[41] L. Yang et al., "Covert transmission and secrecy analysis of RS-RIS-NOMA-aided 6G wireless communication systems," *IEEE Trans. Veh. Technol.*, vol. 72, no. 8, pp. 10659–10670, Aug. 2023.

[42] L. Yang, X. Gao, and M.-S. Alouini, "Performance analysis of relay-assisted all-optical FSO networks over strong atmospheric turbulence channels with pointing errors," *J. Lightw. Technol.*, vol. 32, no. 23, pp. 4613–4620, Dec. 15, 2014.

Xuquan Luo was born in Hunan, China. He received the bachelor's degree from Nanjing University of Aeronautics and Astronautics, Nanjing, China, in 2023. He is currently pursuing the master's degree with the School of Computer Science and Electronic Engineering, Hunan University, Changsha, China. His current research interests include performance analysis of wireless communication systems.

Liang Yang (Senior Member, IEEE) was born in Hunan, China. He received the Ph.D. degree in electrical engineering from Sun Yat-sen University, Guangzhou, China, in 2006. From 2006 to 2013, he was a Teacher with Jinan University, Guangzhou. In 2013, he joined Guangdong University of Technology, Guangzhou. He is currently a Professor with Hunan University, Changsha, China. His current research interests include the performance analysis of wireless communications systems.

George C. Alexandropoulos (Senior Member, IEEE) received the Engineering Diploma (Integrated M.Sc.), M.A.Sc., and Ph.D. degrees in computer engineering and informatics from the School of Engineering, University of Patras, Greece, in 2003, 2005, and 2010, respectively. He held senior research positions at various Greek universities and research institutes, and he was a Senior Research Engineer and a Principal Researcher with the Mathematical and Algorithmic Sciences Laboratory, Paris Research Center, Huawei Technologies France, and the Technology Innovation Institute, Abu Dhabi, United Arab Emirates, respectively. He is currently an Associate Professor with the Department of Informatics and Telecommunications, School of Sciences, National and Kapodistrian University of Athens (NKUA), Greece, and an Adjunct Professor with the Department of Electrical and Computer Engineering, University of Illinois Chicago, Chicago, IL, USA. His research interests include algorithmic design and performance analysis for wireless networks with emphasis on multi-antenna transceiver hardware architectures, full duplex MIMO, active and passive RISs, ISAC, millimeter wave and THz communications, and distributed machine learning algorithms. He is a Senior Member of the IEEE Communications, Signal Processing, Vehicular Technology, and Information Theory Societies, the Chair of the EURASIP Technical Area Committee on Signal Processing for Communications and Networking, and a registered Professional Engineer of the Technical Chamber of Greece. From 2022 to 2024, he was a Distinguished Lecturer of the IEEE Communications Society. He has participated and/or technically managed more than 15 European Union, international, and Greek research, innovation, and development projects, including the H2020 RISE-6G, SNS JU TERRAMETA, SNS JU 6G-DISAC, and ESA PRISM projects dealing with RIS-empowered smart wireless environments, THz RISs, distributed ISAC, and RIS demonstration for localization and mapping, respectively. He was a recipient of the Best Ph.D. Thesis Award 2010, the IEEE Communications Society Best Young Professional in Industry Award 2018, the EURASIP Best Paper Award of the *EURASIP Journal on Wireless Communications and Networking* 2021, the IEEE Marconi Prize Paper Award in Wireless Communications 2021, the Best Paper Awards from the IEEE GLOBECOM 2021 and IEEE VTC-Spring 2025, the Best Paper and Honorable Mention Award 2025 from the *Intelligent and Converged Networks*, the IEEE Communications Society Fred Ellersick Prizes 2023 and 2024, the IEEE Communications Society Leonard G. Abraham Prize 2024, and the NKUA's Research Excellence Award for the academic year 2023–2024. He also serves as an Editor for IEEE TRANSACTIONS ON COMMUNICATIONS, IEEE TRANSACTIONS ON GREEN COMMUNICATIONS AND NETWORKING, IEEE TRANSACTIONS ON MOBILE COMPUTING, IEEE WIRELESS COMMUNICATIONS LETTERS, *Frontiers in Communications and Networks*, and the *ITU Journal on Future and Evolving Technologies*. More information is available at https://www.alexandropoulos.info

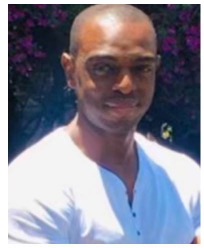

Jules M. Moualeu (Senior Member, IEEE) received the Ph.D. degree in electronic engineering from the University of KwaZulu-Natal, Durban, South Africa, in 2013. During the Ph.D. degree, he was a Visiting Scholar with Concordia University, Montreal, QC, Canada, under Canadian Commonwealth Scholarship Program offered by the Foreign Affairs and International Trade Canada (DFAIT). In 2015, he joined the Department of Electrical and Information Engineering, University of the Witwatersrand, Johannesburg, South Africa, where he is currently an Associate Professor. He was a Visiting Associate Professor with Lappeenranta-Lahti University of Technology, Lappeenranta, Finland, in 2024. From 2018 to 2021, he was an Affiliate Assistant Professor with Concordia University. His current research interests include 5G and 6G enabling technologies, optical wireless communications, reconfigurable intelligent surfaces, and physical layer security in wireless networks. He received the Exemplary Reviewer Award of IEEE COMMUNICATIONS LETTERS from 2018 to 2022 and IEEE TRANSACTIONS ON COMMUNICATIONS in 2021. He served as an Associate Editor for IEEE ACCESS from 2018 to 2023. He is also an Associate Editor of *Frontiers in Communications and Networks* and IEEE TRANSACTIONS ON COGNITIVE COMMUNICATIONS AND NETWORKING, a Senior Reviewer of IEEE OPEN JOURNAL OF THE COMMUNICATIONS SOCIETY, and the Managing Editor of IEEE COMMUNICATIONS LETTERS.

Xi Yang (Member, IEEE) received the B.E. degree in electronic information engineering from Jishou University, Jishou, China, in 2001, the M.E. degree in communication and information system from North China Electric Power University, Baoding, China, in 2004, and the Ph.D. degree in information and communication engineering from the National Mobile Communications Research Laboratory (NCRL), Southeast University, Nanjing, China, in 2014. From 2014 to 2020, he was a Post-Doctoral Fellow with the State Key Laboratory of Millimeter Waves, Southeast University, Nanjing. He is currently a Professor with the School of Communication and Electronic Engineering (SCEE), Jishou University. His current research interests include cognitive radio, smart communication, statistical, and intelligent signal processing.